Energy 332 (2025) 137139

Contents lists available at ScienceDirect

Energy

journal homepage: www.elsevier.com/locate/energy

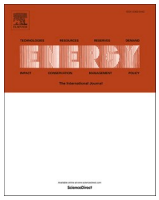

Enhancing the future adaptability of boiler systems using multi-input extremum seeking control algorithms

Tianyu Zhou [a], Chao Yang [a,1], Lijie Wang [a], Yifan Wang [a], Can Zhou [a], Xuesen Pu [c], Zhongcai Zhang [d], Lingxiao Kong [a], Zimu Dong [a], Libin Yu [b], Chang Tan [a], Chenghang Zheng [a,b,*], Xiang Gao [a,b,**]

[a] State Key Lab of Clean Energy Utilization, State Environmental Protection Engineering Center for Coal-Fired Air Pollution Control, Zhejiang University, Hangzhou, 310027, China
[b] Zhejiang Baima Lake Laboratory Co., Ltd., Hangzhou, 310051, China
[c] Dongfang Electric Autocontrol Engineering Co., Ltd., Deyang, 618000, China
[d] Dongfang Boiler Co., Ltd., Chengdu, 610000, China

ARTICLE INFO

Keywords:
Real-time combustion optimization
Extremum seeking control
Air-coal ratio
Multi-objective optimization

ABSTRACT

Traditional boiler control systems demonstrate inherent limitations in sustaining operational efficiency under frequent load fluctuations and alternative fuel co-firing conditions, primarily attributable to open-loop optimization architectures and delayed response to automatic generation control (AGC) signals. This investigation develops a Multi-input Extremum Seeking Control (MESC) algorithm that dynamically optimizes secondary air distribution parameters (specifically auxiliary air/close-coupled over-fire air/separated over-fire air) through a closed-loop Simulink-APROS integration framework, circumventing conventional reliance on prior system modeling. Experimental validation under 1000-900 MW flexible operation scenarios demonstrate a 1.53 % reduction in the composite objective function jointly evaluating coal consumption rate of power supply (CCR) and nitrogen oxide (NO_x) emissions. The proposed method achieves rapid convergence near optimal values within 1800 s even under incomplete combustion and fuel quality disturbances. The algorithm demonstrates effective trade-offs between CCR and NO_x concentration. Under load variation scenarios and coal quality disturbances, it achieves 27 % and 25 % NO_x reductions respectively, while prioritizing optimization of CCR under suboptimal initial operating conditions. Parametric analysis of weighting factors reveals increased coal pricing amplifies prioritization of CCR optimization, necessitating strategic equilibrium between economic objectives and emission constraints. By enabling model-free real-time self-optimization, this novel approach enhances operational resilience of coal-fired units in renewable-penetrated power networks, offering a practical solution to evolving decarbonization mandates.

Nomenclature

Abbreviations	
AA	Auxiliary air
ABS	Anti-lock braking systems
ACR	Air-coal ratio
AGC	Automatic generation control
CCOFA	Close-coupled over-fire air
CCR	Coal consumption rate of power supply
CFD	Computational fluid dynamics
CFPP	Coal-fired power plant
DBN	Deep belief networks
DCS	Distributed control system
DMC	Dynamic matrix control
DRL	Deep reinforcement learning

(continued on next column)

(continued)

(continued on next page)

* Corresponding author. State Key Lab of Clean Energy Utilization, State Environmental Protection Engineering Center for Coal-Fired Air Pollution Control, Zhejiang University, Hangzhou, 310027, China.
** Corresponding author. State Key Lab of Clean Energy Utilization, State Environmental Protection Engineering Center for Coal-Fired Air Pollution Control, Zhejiang University, Hangzhou, 310027, China.
E-mail addresses: zhengch2003@zju.edu.cn (C. Zheng), xgao1@zju.edu.cn (X. Gao).
[1] Co-first author.

https://doi.org/10.1016/j.energy.2025.137139
Received 12 April 2025; Received in revised form 26 May 2025; Accepted 14 June 2025
Available online 16 June 2025

(*continued*)

ESC	Extremum seeking control
FD Fan	Forced draft fan
F-NMPC	Fast nonlinear model predictive control
IC	Initial condition
IEA	International Energy Agency
M_{CCR}	Value of coal consumption rate of power supply
MESC	Multi-input extremum seeking control
MIMO	Multiple-input multiple-output
MPC	Model predictive control
MSHS	Molten salt heat storage system
OC	Optimized condition
OPC	Object linking and embedding (OLE) for process control
PA	Primary air
SA	Secondary air
SCR	Selective catalytic reduction
S-NMPC	Slow nonlinear model predictive control
SOFA	Separated over-fire air
THA	Turbine heat acceptance
T-NMPC	Two-timescale nonlinear model predictive control
VC	Variable condition
Symbols	
B	Coal feed rate
b	Specific standard coal consumption rate of power supply
c_{NO_x}	NO_x concentration (mg/m^3)
$COST_{coal}$	Cost of coal (CNY/kWh)
$COST_{NO_x}$	Cost of NO_x desorption (CNY/kWh)
E_{out}	Power output by the plant (MW)
J_{MESC}	Composite objective function
k	Learning rate (or gain)
M_{CCR}	Value of coal Consumption rate of power supply (g/kWh)
M_p	Overshoot
$M(t)$	Demodulation signal
NO_x	Nitrogen oxide
p	Weighting factors for CCR
$PRICE_{coal}$	Real-time standard coal market price (CNY/t)
$PRICE_{NH_3}$	Liquid ammonia market price (CNY/t)
Q_{air}	Mass flow rate of air entering the boiler (kg/h)
Q_{coal}	Mass flow rate of pulverized coal entering the boiler (kg/h)
Q_{m,NH_3}	Specifies theoretical ammonia demand for NO_x removal per kilowatt
q	Weighting factors for NO_x concentration
$S(t)$	Perturbation signal
T_r	Rise time (s)
T_{ss}	Settling time (s)
$t_{0\ \%}$	The initiation time (s)
$t_{100\ \%}$	The time required to reach steady-state (s)
$u_{ACR_{AA}}$	Value of ACR for auxiliary air
$u_{ACR_{CCOFA}}$	Value of ACR for close-coupled over-fire air
$u_{ACR_{SOFA}}$	Value of ACR for separated over-fire air
V_{gv}	Dry flue gas volume
Y_p	The output peak value
Y_{ss}	The steady-state value
$y(t)$	Measurements of the control system
β	Ammonia-nitrogen ratio
θ_{AA}	Value of the air-coal ratio of auxiliary air as an uncertain parameter
θ_{CCOFA}	Value of the air-coal ratio of close-coupled over-fire air as an uncertain parameter
θ_{SOFA}	Value of the air-coal ratio of separated over-fire air as an uncertain parameter
$\widehat{\theta}_{AA}$	Estimated value of the air-coal ratio of auxiliary air as an uncertain parameter
$\widehat{\theta}_{CCOFA}$	Estimated value of the air-coal ratio of close-coupled over-fire air as an uncertain parameter
$\widehat{\theta}_{SOFA}$	Estimated value of the air-coal ratio of separated over-fire air as an uncertain parameter
ω	Signal frequency

1. Introduction

The global energy system currently grapples with a fundamental dilemma: reconciling carbon neutrality objectives with escalating electricity demands. The challenge lies in developing localized solutions that ensure clean, efficient, and low-carbon energy operations. International Energy Agency (IEA) [1] data reveals that Chinese power plants contributed approximately one-third of global coal consumption for electricity generation in 2024. China's electricity sector, shaped by its unique resource endowment characterized by abundant coal reserves, limited oil resources, and constrained natural gas supplies, remains a pivotal driver of international coal market dynamics. Coal-fired generation constitutes nearly 40 % of the nation's total electricity production capacity, with projections indicating that CO_2 emissions from energy combustion and industrial processes will peak at approximately 12.2 gigatonnes between 2028 and 2029 [2]. Recent technological advancements have enabled Chinese coal-fired units to achieve operational excellence, demonstrated by a reduction in standard coal consumption rate to 301.6 g/kWh. However, emerging challenges threaten these efficiency gains. Increasingly frequent load variation requirements and policy-driven integration of renewable energy sources are eroding the performance advantages of conventional coal-fired units, manifesting in elevated and unstable coal consumption patterns. This operational instability underscores the critical need for innovative control algorithm development to maintain generation efficiency under complex variable-load conditions, a persistent technical hurdle demanding urgent resolution.

Conventional coal-fired power plants (CFPP) typically operate in steady-state conditions for prolonged durations, maintaining stable parameters through minimal manual intervention while their output power is directly regulated by grid Automatic Generation Control (AGC) systems. These commands are processed through the Distributed Control System (DCS), which calculates and transmits corresponding coal feed instructions to mills. Operators typically perform minor Air-Coal Ratio (ACR) adjustments based on flue gas oxygen feedback and empirical knowledge to maximize boiler efficiency. However, the grid penetration of renewable energy has compelled coal-fired units to assume primary responsibility for balancing the inconsistency and mismatch of stochastic power fluctuations. This transition has exposed critical limitations in traditional control systems, particularly their phase delay characteristics and open-loop optimization deficiencies. Reliance on manual adjustments introduces substantial load deviations, resulting in non-compliance with AGC commands that triggers grid penalties and escalates operational costs.

To address these challenges, numerous system optimization methodologies have emerged. Hentschel et al. [3] developed a control-physics co-simulation framework in APROS to identify control loop bottlenecks and design compensation mechanisms under grid frequency regulation demands, achieving maximized dynamic response capacity within safety boundaries. Hubel et al. [4] created a dynamic simulation model that replicates plant startup processes while balancing thermal and mechanical stress constraints, significantly reducing fuel consumption and emissions. Kusiak et al. [5,16] established an offline optimization model targeting boiler efficiency improvements through heat rate and coal consumption analysis, identifying key combustion parameters for operational guidance. Existing studies on coal-fired power plant dynamic simulations further demonstrate diverse operational scenarios and performance metrics [6–9]. Regarding advanced control algorithms, Dai et al. [10] developed a predictive control framework (PMA-OC) integrating model predictive control with deep reinforcement learning, utilizing low-fidelity modeling for initial system coordination and continuous DRL optimization to achieve enhanced interference rejection, dynamic response, and control precision beyond standalone approaches. Zhu et al. [11] developed a three-term MPC strategy that effectively addresses oscillation suppression and rapid response challenges in large-delay systems. Ashraf et al. [12] employed extreme learning machines and support vector regression for plant data modeling, coupled with response surface methodology for operational parameter optimization, achieving measurable improvements in fuel utilization efficiency, thermal efficiency, and reductions in CO_2/CH_4 emissions. In CFPP integrated with molten salt thermal storage systems, Cui et al. [13] developed a predictive control system employing Dynamic Matrix Control (DMC) algorithms to coordinate steam extraction valve openings and molten salt pump flow rates, achieving significant improvements in both transient response and operational stability. For

carbon capture-equipped CFPP, Liao et al. [14] pioneered a two-tiered control architecture: the scheduling tier utilizes Deep Belief Networks (DBN) coupled with Bayesian optimization to dynamically determine economically optimal setpoints for power generation and carbon capture, while the execution tier implements Model Predictive Control (MPC) for multivariable tracking. This hierarchical structure enables simultaneous compliance with 50 %–90 % carbon capture requirements and economic dispatch objectives under electricity price volatility. Yang et al. [15] addressed dynamic response time discrepancies in flexible control of coal-fired power plants by developing a two-timescale nonlinear model predictive control strategy (T-NMPC). This approach integrates coordinated optimization between slow (S-NMPC) and fast (F-NMPC) controllers, demonstrating significant enhancements in both AGC response rate and control accuracy.

While plant-wide optimization methods have been extensively studied, computational fluid dynamics (CFD) has been conventionally applied to analyze boiler combustion processes. Notably investigated by Shi et al. [17–19] for combustion optimization, this approach remains fundamentally constrained by time-intensive modeling processes involving boundary configuration and computational demands, limiting practical implementation for real-time optimization while exhibiting strong model dependency. This rationale underlies our proposal of a model-free multi-input extremum seeking control (MESC) algorithm. Originating from Leblanc's pioneering work in the 1920s [20], extremum seeking control (ESC) gained practical significance in late 20th-century engineering applications [21,22], now extensively implemented in automotive anti-lock braking systems (ABS) [23] and photovoltaic maximum power point tracking [24]. Confronting increasingly unpredictable operational conditions, modern boiler combustion systems demand adaptive self-optimizing capabilities. Modern boiler combustion control systems require self-adaptive and self-optimizing capabilities to address uncertain future operating conditions. The proposed algorithm achieves extremum seeking without relying on prior knowledge of boiler input-output mappings while maintaining system operation near the optima of predefined objective functions. This approach demonstrates particular effectiveness in governing nonlinear, strongly coupled thermodynamic systems characteristic of industrial boilers. The self-optimization capability of ESC fundamentally depends on real-time optimization, a well-established research area [25–28]. Zhu et al. [29] advanced a system identification-based method to refine gradient estimation in model-free scenarios, demonstrating effective optimization for high-efficiency and low-emission unit operations, which offers methodological relevance to this study. Practically, Marjanovic et al. [30] implemented ESC to optimize burner configurations in a 350 MW Serbian boiler, achieving enhanced combustion efficiency and reduced furnace wall degradation. A key limitation of these prior studies lies in their data dependency: model identification methods require extracting information from substantial historical data to construct models, while popular offline learning approaches (e.g., DRL) necessitate historical datasets for pre-training. These procedures are time-consuming and data quality-dependent, hindering rapid online optimization objectives. In contrast, MESC, as a model-free optimization method, circumvents model mismatch issues and exhibits superior robustness in noise-intensive scenarios such as coal quality disturbances.

Boilers represent typical multiple-input multiple-output (MIMO) systems where isolated single-variable control strategies prove inadequate in meeting operational demands, often resulting in poor coordinated regulation outcomes. While multi-objective optimization has been extensively explored in scenarios like integrated energy systems [31–34], exemplified by Li's application of a multi-objective grey wolf optimization algorithm to balance exergy efficiency and Molten Salt Heat Storage System (MSHS) round-trip efficiency, such approaches remain non-trivial in boiler control contexts. This study investigates a 1000 MW ultra-supercritical power generation unit, performing multi-objective optimization between coal consumption per kilowatt-hour and nitrate oxide concentration [35], while extending the existing algorithmic framework of using ESC for single-variable optimization problems.

This work proposes a boiler combustion air distribution system employing a multi-input extremum seeking control (ESC) algorithm, which optimizes layered air distribution through key combustion-influencing variables while balancing boiler efficiency and emission constraints. A boiler combustion and air distribution testbed was developed using APROS THERMAL 6 to implement and validate system-level operational strategies through dynamic simulations. The ESC demonstrated enhanced optimization capabilities under flexible operation modes, coal quality disturbances, and complex combustion scenarios, achieving optimization values faster than conventional methods with improved adaptability to high fluctuation conditions. Fuel price sensitivity analysis further revealed the necessity of context-specific weight factor selection in composite objective functions.

2. Establishment of the test environment for boiler combustion and auxiliary system

The case study focuses on a 1000 MW ultra-supercritical single-reheat condensing steam unit with minimum stable combustion capability at 30 % Turbine Heat Acceptance (THA) load. This integrated system comprises core subsystems including combustion regulation, air volume control, coal feed management, and feedwater supply. Its thermal recovery configuration incorporates three-stage high-pressure heaters, three-stage low-pressure heaters, and a deaerator. The unit performs real-time power output adjustments in response to Automatic Generation Control (AGC) commands through a continuously active closed-loop electric load regulation mechanism. The forced draft air system bifurcates into primary air (PA) and secondary air (SA) streams. PA undergoes preheating before entering the mill for coal-air mixture preparation and temperature modulation prior to furnace injection. SA constitutes the dominant airflow component, directly supplying combustion oxygen through multiple functional layers: auxiliary air (AA), close-coupled over-fire air (CCOFA) and separated over-fire air (SOFA).

The primary control objectives focus on optimizing two critical operational parameters: Coal consumption rate of power supply (CCR) and NO_x emission levels. Achieving these targets requires precise regulation of combustion airflow distribution, necessitating the development of high-fidelity models for the air supply control architecture. Figs. 1 and 2 illustrates both the operational workflow of the coal-fired unit and the comprehensive boiler system model implemented in APROS THERMAL 6 simulation environments. In Fig. 2, steam & water conduits are highlighted in blue fluorescence, while combustion circuits (air & flue gas) are marked in orange fluorescence. Heat exchange between the two circuits is achieved through radiative heat exchangers, convective heat exchangers, explicitly illustrating the thermal transfer process.

Model validation was conducted through comparative analysis between simulated outputs and actual thermal process data under closed-loop operational conditions, as detailed in Table 1. The verification demonstrates prediction errors within statistically bounded margin, thereby enabling subsequent experimental investigations (see Table 2).

3. Design of boiler combustion systems equipped with MESC algorithms

3.1. Optimization problem formulation

Detailed analysis of boiler combustion systems reveals significant correlations between control objectives and total airflow volume. The unit's specific coal consumption rate of power supply exhibits a non-monotonic dependence on airflow rate, initially decreasing through combustion efficiency enhancement before gradually increasing beyond optimal thresholds. This phenomenon arises from competing thermodynamic mechanisms: moderate airflow improves pulverized coal

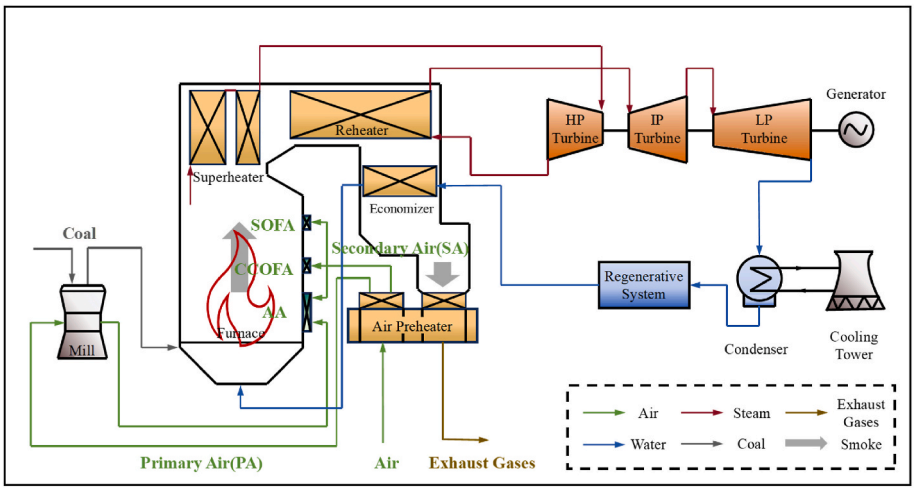

Fig. 1. Schematic diagram of coal-fired power unit.

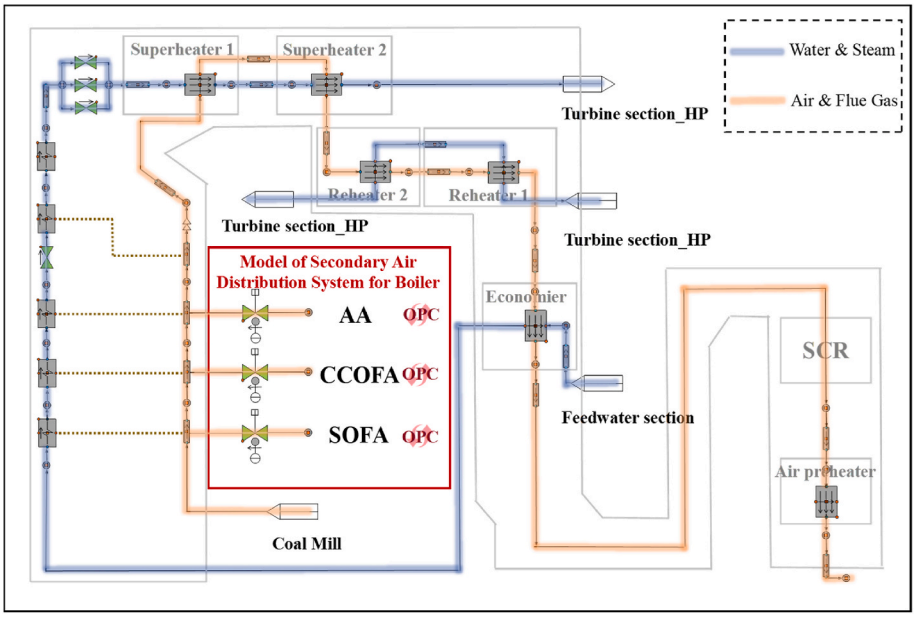

Fig. 2. Boiler System and air distribution system modelled in APROS THERMAL 6.

Table 1
Comparison between the real and simulation values at steady condition (the real values were obtained from operational units under 1000 MW rated conditions).

Parameter	Unit	Simulation value	Real value	Errors
Coal feed rate	t/h	409.32	408.77	0.13 %
Superheated steam pressure	MPa	26.56	26.56	0 %
Superheated steam temperature	°C	592.70	593.96	0.21 %
Total air flow	t/h	3151.76	2934.8	7.39 %
Primary air flow	t/h	759.29	781.22	2.81 %
Oxygen content in flue gas	%	3.65	3.62	0.83 %

combustion efficiency, while excessive volumes reduce combustion chamber temperatures and amplify flue gas heat losses, thereby increasing coal consumption.

Nitrogen oxide (NO_x) formation exhibits direct dependence on staged air distribution strategies. The formation of nitrogen oxides (NO_x) in boilers is directly influenced by stratified air distribution configurations. Under fixed air distribution ratios across combustion zones, NO_x concentration has the characteristic of a function with a minimum relative to total air volume—a phenomenon well-documented in experimental and theoretical studies [36,37]. This behavior stems from two mechanisms: fuel NO_x dominates in oxygen-deficient environments, while thermal NO_x prevails under oxygen-enriched combustion conditions. Consequently, a comprehensive objective function incorporating multiple control variables enables multi-objective optimization in complex combustion scenarios, with identifiable optimal operating points as illustrated in Fig. 3.

Following this research approach, the initial step involves defining input decision variables. In practical power plant operations, real-time adjustments to air distribution primarily rely on optimizing the air-coal ratio. Given that secondary air constitutes a major proportion of total airflow and plays a decisive role in combustion processes, while its stratified distribution pattern significantly influences real-time nitrate oxide concentrations, three secondary air parameters are selected as decision variables: auxiliary air (AA), close-coupled over-fire air (CCOFA), and separated over-fire air (SOFA). The auxiliary air supplies the majority of oxygen required for combustion while regulating

Table 2
Multi-input optimization effects for variable load condition.

	Load (MW)	ACR_{AA}	ACR_{CCOFA}	ACR_{SOFA}	NO_x (mg/m^3)	CCR (g/kWh)	J_{MESC}
IC	1000	3.50	1.26	1.09	366.92	280.10	284.45
OC	1000	2.14	1.37	2.30	267.96	280.70	280.10
VC1	950	2.40	1.38	2.31	278.49	277.81	277.88
VC2	900	2.09	1.38	2.37	263.04	271.33	270.91
VC3	1000	1.83	1.37	2.60	246.32	280.80	279.04

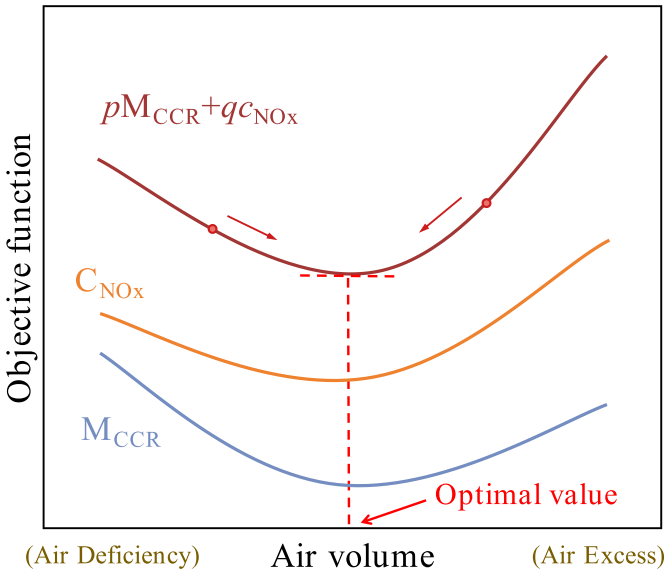

Fig. 3. Qualitative characterization curves for multi-objective optimization of boiler combustion.

turbulent flow distribution to enhance combustion conditions. Close-coupled over-fire air (CCOFA) facilitates the combustion of residual fuel, thereby further reducing NOx concentrations and simultaneously mitigating slag formation on water-cooled walls above burners. Separated over-fire air (SOFA) ensures complete fuel burnout while effectively reducing carbon content in fly ash, CO_2 emissions, and suppressing NO_x generation. From the control system perspective, the multivariable extremum seeking control algorithm design consequently incorporates three system inputs (as illustrated in Fig. 4).

The subsequent critical task involves formulating the objective function through comprehensive multi-criteria analysis of boiler combustion dynamics. As previously established, the control objectives focus on optimizing two pivotal operational indicators: specific coal consumption per kilowatt-hour and nitrogen oxide (NO_x) concentration. These parameters fundamentally determine boiler operational efficiency and environmental compliance, while their optimization effectiveness serves as the primary adaptability evaluation metric for system evolution. The composite objective function can thus be mathematically expressed as:

$$J_{MESC} = pM_{CCR} + qc_{NO_x}$$

$$s.t.\begin{cases} p+q=1 \\ p=\dfrac{\mathrm{COST_{coal}}}{\mathrm{COST_{coal}}+\mathrm{COST_{NO_x}}} \\ q=\dfrac{\mathrm{COST_{NO_x}}}{\mathrm{COST_{coal}}+\mathrm{COST_{NO_x}}} \end{cases} \quad (1)$$

The objective function incorporates weighting factors p and q for specific coal consumption rate of power supply and NO_x concentration respectively. These coefficients are functionally dependent on the economic weighting between fuel expenditure and denitrification operational costs, with their respective cost calculations governed by:

$$\mathrm{COST_{coal}} = b \times \frac{\mathrm{PRICE_{coal}}}{10^6} \quad (2)$$

where b is specific standard coal consumption rate of power supply (g/kWh) and $PRICE_{coal}$ is the real-time standard coal market price (CNY/t).

$$\mathrm{COST_{NO_x}} = c_{NO_x} \times B \times V_{gv} \times Q_{m,NH_3} \times \beta \times \mathrm{PRICE_{NH_3}} \quad (3)$$

The formulation parameters are defined as follows: c_{NOx} denotes boiler outlet NO_x concentration (mg/m^3). B represents coal feed rate (t/h). V_{gy} indicates dry flue gas volume (m^3/kg). $Q_{m,NH3}$ specifies theoretical ammonia demand for NO_x removal. β corresponds to ammonia-nitrogen ratio and $PRICE_{NH3}$ reflects liquid ammonia cost (CNY/t). Operational analysis with standard coal priced at 1000 CNY/t yields calculated fuel cost at 0.28 CNY/kWh and denitrification cost at 0.0147 CNY/kWh, resulting in weighting coefficients $p = 0.95$ and $q = 0.05$ through economic prioritization.

The air-coal ratio (ACR) is a critical parameter for combustion regulation in power plants, as formally defined in Eq. 4.Q_{air} and Q_{coal} represent the mass flow rate of air and pulverized coal entering the boiler (kg/h). Clearly, the air supply magnitude is reflected in the ACR. Subsequent analyses uniformly adopt the ACR of three secondary air as input parameters.

$$u_{ACR} = \frac{Q_{air}}{Q_{coal}} \quad (4)$$

Additionally, operational adjustments to ACR in practical boiler systems are subject to inherent operational boundaries. Exceeding these thresholds incurs substantial efficiency penalties, necessitating constrained optimization within the objective function's feasible domain. The implemented constraints serve dual purposes: restricting the algorithm's search space to physically viable regions while preventing premature convergence to local optima and improving robustness against modeling inaccuracies. This constrained optimization framework ensures enhanced operational adaptability across variable conditions and provides inherent safeguards for future complex operational scenarios. The ACR must therefore maintain fluctuations within the following operational envelope:

$$u_{ACR_{AA}\ min} < u_{ACR_{AA}} < u_{ACR_{AA}\ max} \quad (5)$$

$$u_{ACR_{CCOFA}\ min} < u_{ACR_{CCOFA}} < u_{ACR_{CCOFA}\ max} \quad (6)$$

$$u_{ACR_{SOFA}\ min} < u_{ACR_{SOFA}} < u_{ACR_{SOFA}\ max} \quad (7)$$

In the formula, $u_{ACR_{AA}}$, $u_{ACR_{CCOFA}}$, $u_{ACR_{SOFA}}$ represent the ACR for auxiliary air, close-coupled over-fire air and separated over-fire air respectively. The normal operating ranges for these ACR are defined as follows: $u_{ACR_{AA}\ min}$ and $u_{ACR_{AA}\ max}$ for AA, $u_{ACR_{CCOFA}\ min}$ and $u_{ACR_{CCOFA}\ max}$ for CCOFA, $u_{ACR_{SOFA}\ min}$ and $u_{ACR_{SOFA}\ max}$ for SOFA. The constraint boundaries are established through rigorous analysis of historical plant operational data, primarily anchored in two critical operational parameters: the plant's permissible tolerance range for ACR and the safety margins of auxiliary equipment. These metrics are directly related to operational costs and safety, most accurately reflecting the plant's practical requirements.

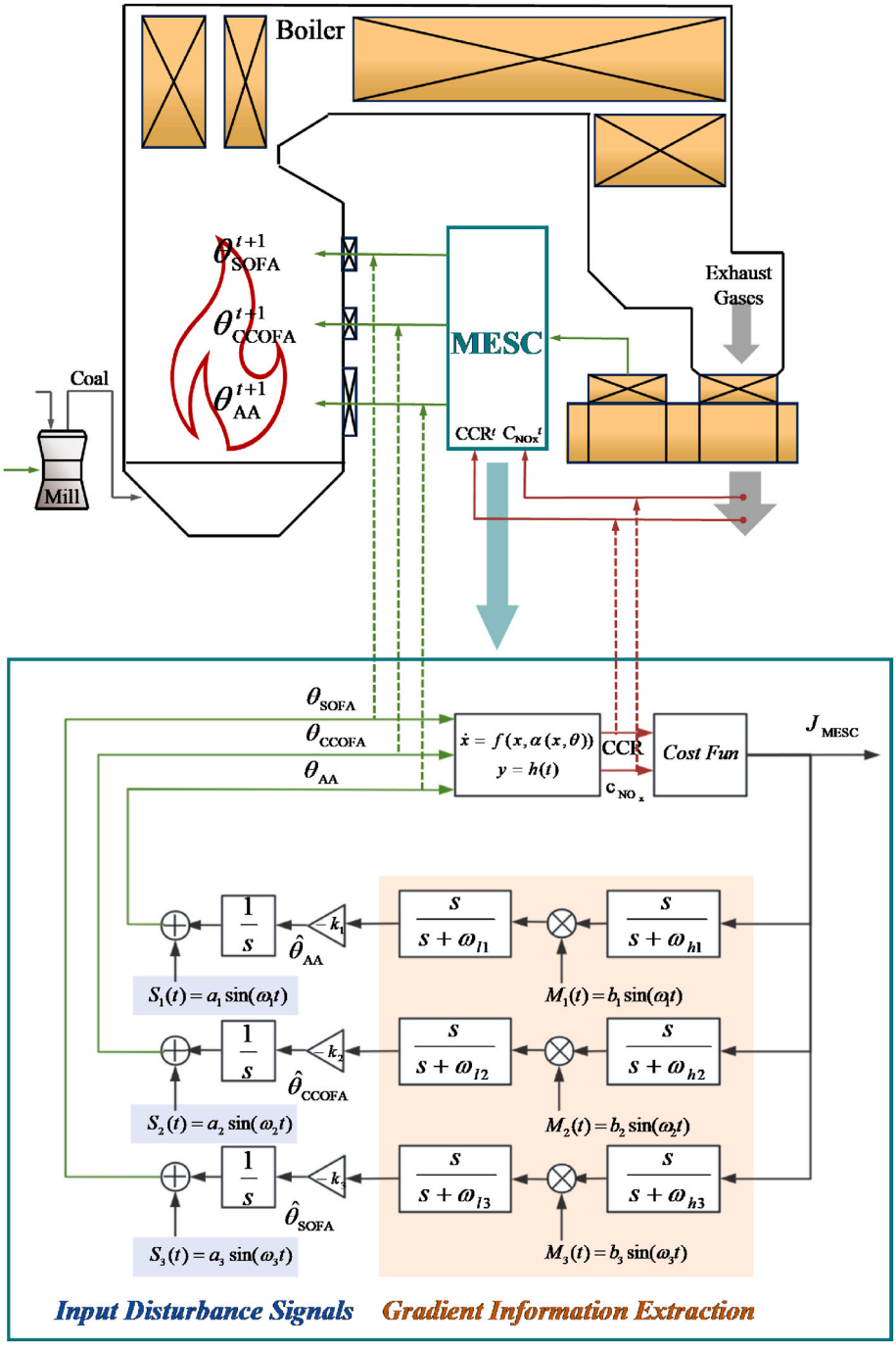

Fig. 4. Logic diagram of MESC algorithm.

3.2. Implementation strategies for MESC algorithms

Extremum seeking control operates through gradient-based optimization, autonomously adjusting control parameters via continuous performance metric evaluation. For the boiler, a dynamic system with multivariable nonlinear mapping, the basic control structure is shown in Fig. 4. The perturbation signal $S(t)$ and demodulation signal $M(t)$ are set as follows:

$$S(t) = \begin{bmatrix} a_1 \sin(\omega t) \\ a_2 \sin(\omega t) \\ a_3 \sin(\omega t) \end{bmatrix} \tag{8}$$

$$M(t) = \begin{bmatrix} b_1 \sin(\omega t) \\ b_2 \sin(\omega t) \\ b_3 \sin(\omega t) \end{bmatrix} \tag{9}$$

The perturbation frequencies should satisfy the following conditions [38] ($i \neq j \neq k$):

1) All pairwise perturbation frequencies are distinct ($\omega_i \neq \omega_j$);
2) The ratio of any two frequencies is a rational number ($\omega_i/\omega_j \in Q$);
3) The sum of any two frequencies does not equal a third frequency ($\omega_i + \omega_j \neq \omega_k$).

It is crucial that the perturbation frequencies ensure sufficient

temporal separation between the extremum seeking loop and the controlled process.

The control logic's operational principle comprises two fundamental phases: under unknown boiler system dynamics, a low-amplitude periodic perturbation signal is injected into the ACR estimation vector. Subsequent gradient estimation through output response analysis enables parameter optimization via iterative adaptation. Mathematically, the modulation stage introduces a persistent excitation signal to the controller's parameter vector.

$$u(t) = u_0 + a\sin(\omega t) \tag{10}$$

The perturbation introduces coherent frequency-modulated components into the system's performance index, where phase characteristics encode directional gradient information of the performance surface. Following perturbation injection, the perturbed system output y(t) is measured. A high-pass filter subsequently isolates high-frequency components from the output signal. Synchronous demodulation multiplies this filtered signal with the original perturbation waveform, followed by low-pass filtering to extract fundamental frequency constituents, thereby generating real-time gradient estimates of the performance index relative to control parameters.

$$y(t) = \frac{2}{a}\int_0^t y(\tau)\sin(\omega\tau)d\tau \tag{11}$$

Following the gradient descent method and repeating these steps continuously, the system's optimal value is eventually obtained.

$$u_0(t+1) = u_0(t) - ky(t) \tag{12}$$

Fig. 5 schematically illustrates the theoretical framework. The algorithm's optimization entails continuous gradient-based minimization of the composite objective function. Iterative convergence toward optimal regions occurs when parameter estimates remain within the true value's confidence interval. Krstic's [39] stability analysis demonstrates that timescale separation between perturbation frequency and system dynamics guarantees semi-global uniform ultimate boundedness in closed-loop operation. Crucially, this approach eliminates dependency on complex process modeling through direct utilization of measurable performance metrics-a fundamental methodological advantage.

Fig. 6 demonstrates the operational control framework implementing the MESC algorithm in simulations. Following the AGC command dispatch from the power grid, the boiler and turbine control systems implement coordinated yet decoupled adjustments. The schematic diagram explicitly segregates both subsystems, with the boiler system serving as the primary focus of this study. The brown sections retain feedback control loops regulated by AGC commands and flue gas oxygen levels, while the red portions replace manual open-loop optimization with real-time optimization modules driven by composite objective functions. This configuration ensures hierarchical control independence: upper-level modules prioritize maintaining main steam temperature/pressure stability, whereas the MESC modules perform independent optimization. The architecture isolates steam-water parameter influences on optimization objectives, effectively restricting key variables to ACR.

Fundamentally, the ESC mechanism governs three secondary air fans through distinct signal frequencies, with multi-input dynamics resolved via linear superposition of independent signal channels. Unlike DRL methods requiring multi-directional trial-and-error, MESC executes constrained directional optimization, eliminating coupling between parameters. Unrestricted optimization could impose stochastic penalty costs in plant operations.

As a closed-loop control architecture, MESC necessitates real-time boiler parameter monitoring and instantaneous optimization feedback. This implementation requires OPC communication between Simulink and APROS platforms. Within Simulink, mechanism-correction parameters are embedded in each control loop, serving to refine control model adaptability across variable initial conditions, enhance the ACR's responsiveness to objective function dynamics, and accelerate algorithm convergence. The corresponding software integration architecture is illustrated in Fig. 7. To further clarify, the three secondary air streams demonstrate linear coupling characteristics as previously stated, wherein parameter selection and configuration within the control structure impose no adverse effects on algorithmic convergence. During extremum-seeking operations, multiple ACR parameter sets can be identified within the solution space, all fulfilling the extremum optimization requirements of the composite objective function. Consequently, redundant parameter tuning procedures are intentionally excluded from presentation.

4. Effects and discussion on typical combustion conditions

4.1. Optimization effectiveness during flexible operation of power generation units

Flexible operational modes expose coal-fired units to frequent load variations, where conventional control systems exhibit delayed response characteristics in parameter adjustment precision. This operational limitation induces sustained oscillations in core combustion parameters, resulting in combustion instability. Furthermore, non-compliance with

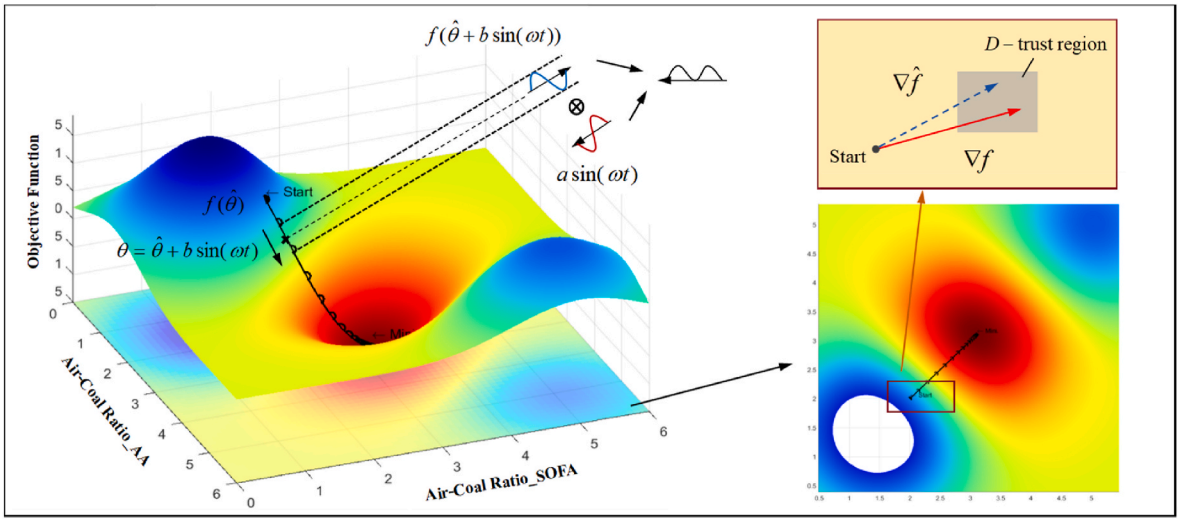

Fig. 5. The gradient descent process of the extremum seeking control algorithm.

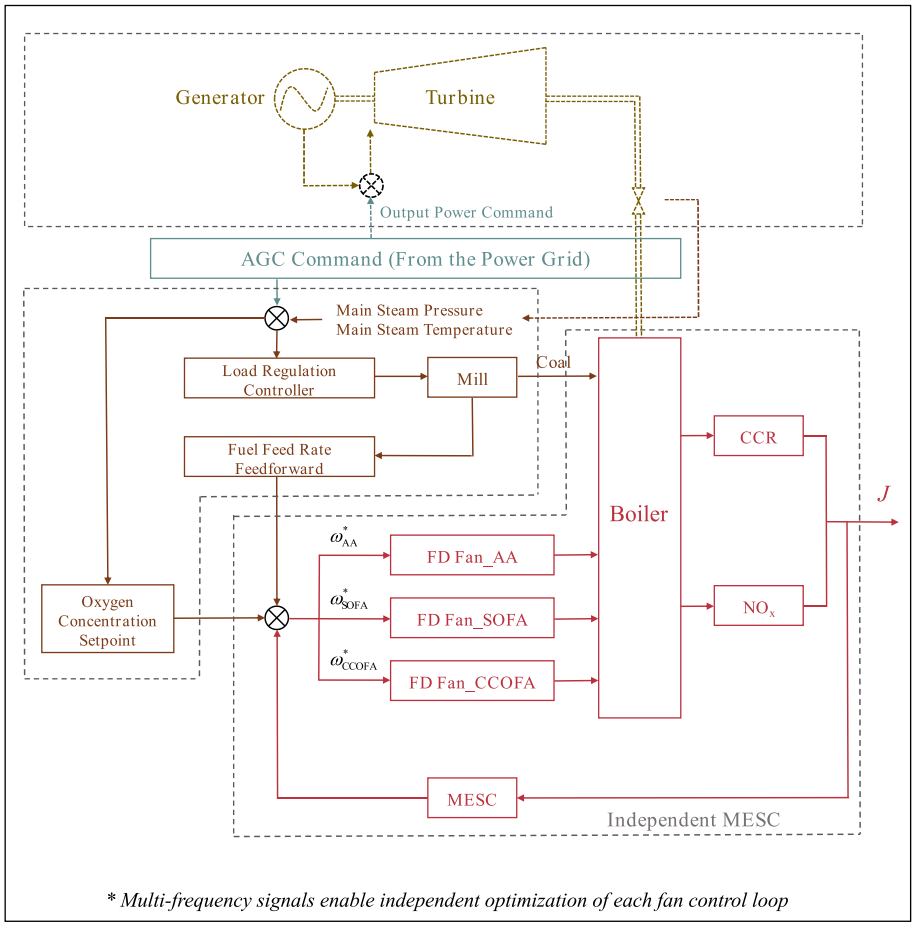

Fig. 6. MESC-based combustion air distribution control system for boilers.

AGC dispatch commands incurs substantial economic penalties through grid-imposed load deviation fines. Consequently, adaptive control algorithms capable of rapid air-fuel ratio optimization become critical for renewable-integrated power systems requiring dynamic boiler responsiveness.

Simulation protocols implement load modulation through AGC command adjustments, necessitating real-time ACR re-optimization during transient conditions. The first diagram in Fig. 8 illustrates the grid-mandated power generation setpoints: 1000 MW → 950 MW → 950 MW → 1000 MW, with E_{out} representing the model's actual generated power output. This establishes the boundary scenario framework for subsequent load-varying scenario optimizations. Crucially, this also implies that MESC operates as a relatively independent optimization subsystem with lower execution priority than maintaining unit power output and steam parameters, embodying a hierarchical optimization approach.

Field-calibrated furnace optimization parameters initialize the simulation model through total air volume input as depicted in Fig. 8 and Table 2. The system initially stabilizes with suboptimal combustion characteristics: coal consumption rate at 280.1 g/kWh and elevated NO_x concentration of 366.92 mg/m^3 under baseline air-coal ratios of ACR_{AA} = 3.5, ACR_{CCOFA} = 1.26 and ACR_{SOFA} = 1.09. Following control system activation at t_1, convergence occurs by t_2 with marginal CCR increase to 280.7 g/kWh alongside 27 % NO_x reduction to 267.96 mg/m^3, accompanied by optimized air ratios of 2.14, 1.37 and 2.30 respectively.

The total air volume remained essentially constant across four optimization cycles. Through strategic air distribution adjustments, the composite objective function ($J_{MESC} = pM_{CCR} + qc_{NO_x}$) that reflects cumulative optimization effects achieved reduction.

It should be emphasized that deep peak shaving scenarios were excluded from this simulation scope. The operational priority for ultra-supercritical units focuses on maintaining generation stability to preserve their inherent efficiency advantages, rather than exclusively serving renewable energy integration objectives.

During three distinct load-variation simulations with differing rate profiles, the ACR solution sets demonstrated remarkable consistency across load change rates. The control architecture exhibited only minor adjustments in ACR_{AA} parameters, confirming model stability under variable conditions. Analysis showed that the J_{MESC} metric at t_8 reached 279.04 g/kWh, indicating improvements over both the baseline and intermediate optimized states. This result demonstrates effective multi-objective optimization.

4.2. Optimization effectiveness under complex scenarios

4.2.1. High CCR and high NO_x scenario

Under conditions of ACR mismatches and combustion temperature anomalies, simultaneous occurrences of elevated coal consumption and high-concentration pollutant emissions may arise. The simulation implements field-derived operational data reflecting inefficient combustion conditions (CCR = 284.70 g/kWh, NO_x = 337.65 mg/m^3) as initial parameters, visualized in Fig. 9(a). Initial air-coal ratios register at ACR_{AA} = 2.8, ACR_{CCOFA} = 1.75 and ACR_{SOFA} = 1.75. Following control system activation at t_1, gradient-based optimization progressively modulates these ratios to 1.87, 1.44 and 2.31 respectively, achieving measurable emission reductions (NO_x = 313.48 mg/m^3) and efficiency gains (CCR = 280.68 g/kWh) within 500 s. This corresponds to 1.81 % reduction in the composite objective function, reaching complete convergence by t_2.

The optimization sequence demonstrates phased implementation:

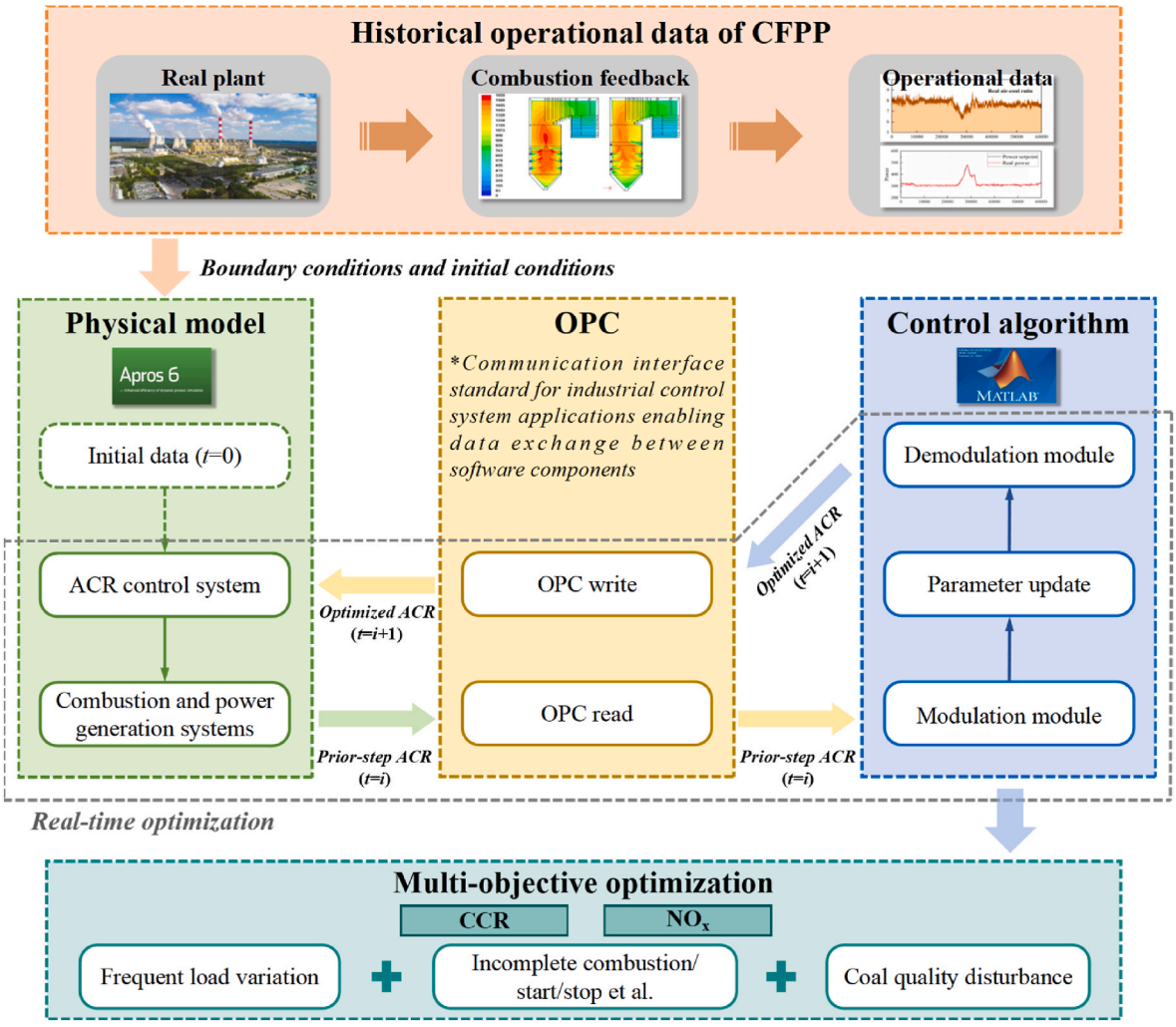

Fig. 7. The Apros model achieves communication with the algorithm implemented in Simulink.

total air volume first stabilizes at ideal levels, followed by layered air distribution refinement. This systematic approach transitions system operation from high-consumption/high-emission states to optimized low-consumption/low-emission performance, with detailed parameter evolution documented in Table 3.

4.2.2. High CCR and low NO_x scenario

Fig. 9(b) illustrates the initial air-coal ratios of $ACR_{AA} = 2.1$, $ACR_{CCOFA} = 2.66$, and $ACR_{SOFA} = 1.05$. Following control system activation at t_1, these parameters underwent rapid adjustment to 2.13, 1.58 and 2.65 respectively, followed by progressive refinement until full convergence. The enhanced separated overfire air volume improved furnace combustion completeness, reducing specific coal consumption from 280.47 g/kWh despite transient NO_x concentration elevation caused by air distribution restructuring. After approximately 1000 s of operational fluctuation, the system stabilized with NO_x levels at 292.37 mg/m^3 and CCR at 280.47 g/kWh, achieving full convergence by t_2 after 1900 s of optimization, as detailed in Table 4.

Although furnace exit NO_x concentration increased from 254.34 mg/m^3 to 292.37 mg/m^3, it remained within acceptable operational thresholds. The composite objective function J_{MESC} decreased by 0.29 %, confirming the cost-effectiveness of this optimization strategy through measurable multi-objective improvement.

4.2.3. Low CCR and high NO_x scenario

Fig. 9(c) demonstrates initial combustion stoichiometry parameters of $ACR_{AA} = 3.5$, $ACR_{CCOFA} = 1.26$ and $ACR_{SOFA} = 1.09$. Following control system activation at t_1, rapid aerodynamic adjustments modulated these ratios to 2.15, 1.36 and 2.37 respectively, initiating progressive optimization until full convergence. The enhanced burnout air ratios precipitated immediate NO_x concentration reduction from 366.90 mg/m^3 to 272.68 mg/m^3, followed by transient concentration fluctuations. Concurrently, layered air distribution modifications during APROS simulation iterations induced combustion efficiency variations, manifesting as CCR oscillations between 280.09 g/kWh and 280.54 g/kWh over 1500 s. Full system stabilization occurred at t_2 after 2300 s of continuous optimization, with detailed parametric evolution documented in Table 5.

While specific coal consumption showed a slight increase, the composite objective function J_{MESC} achieved a 1.48 % reduction. This statistically significant improvement confirms the optimization strategy's cost-effectiveness and operational acceptability.

As shown in Fig. 10, the three scenarios with identical parameters (except initial conditions) were evaluated using standard control metrics: overshoot, rise time, and settling time. Overshoot (M_p) is defined as the maximum percentage deviation by which the output first exceeds the steady-state value relative to that steady-state value. Rise time (T_r) is the time required for the output to increase from 0 % to 100 % of the steady-state value. Settling time (T_{ss}) is the minimum time required for the system response to enter and remain within a ±2 % tolerance band around the steady-state value. Formulae are as follows.

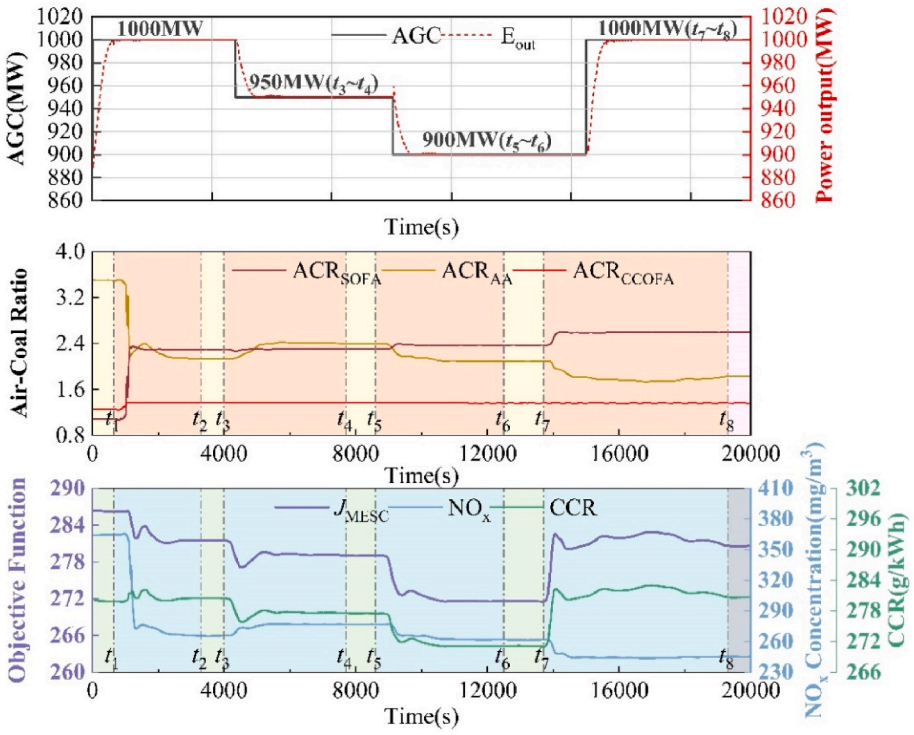

Fig. 8. AGC boundary conditions and optimization control process for variable load condition (*AGC* represents the output power command from AGC).

$$M_p = \frac{Y_p - Y_{ss}}{Y_{ss}} \times 100\% \tag{13}$$

$$T_r = t_{100\%} - t_{0\%} \tag{14}$$

$$T_{ss} = min\left\{ t | \forall \tau > t, \left| \frac{Y(\tau) - Y_{ss}}{Y_{ss}} \right| \leq 2\% \right\} \tag{15}$$

Here, Y_p denotes the output peak value, Y_{ss} the steady-state value, $t_{100\ \%}$ the time required to reach steady-state, $t_{0\%}$ the initiation time and τ a specific time instance. The MESC algorithm exhibits faster response and stabilization than conventional methods, with acceptable system oscillations and reduced ACR overshoot. Additional detailed data and advantages are presented in Fig. 10 and Table 6.

4.2.4. Coal quality disturbance scenario

The increasing adoption of biomass co-firing and alternative green fuels necessitates advanced boiler control systems capable of maintaining operational stability under dynamic fuel composition variations. Conventional coal-quality monitoring systems exhibit significant measurement latency, severely limiting control responsiveness during fuel transitions. The MESC algorithm demonstrates superior adaptability in such scenarios, achieving operational stabilization near optimal conditions within approximately 1800 s during coal-quality fluctuations. This performance significantly surpasses conventional adjustment methods that require multi-hour durations for preliminary tuning and combustion observation.

Fig. 9(d) illustrates system performance under simulated coal quality disturbances at 950 MW load, implemented through historical NO_x concentration step-changes. At t_1, an instantaneous NO_x reduction from 370 mg/m^3 to 323 mg/m^3 triggers J_{MESC} decline to 282.46. Subsequent optimization over 3500 s yields stabilized ACR: $ACR_{AA} = 2.63$, $ACR_{C\text{-}COFA} = 1.71$ and $ACR_{SOFA} = 1.63$, representing adjustments from initial 3.02, 1.70, and 1.34 respectively. The final $J_{MESC} = 279.02$ reflects 1.21 % reduction from the step-change reference, demonstrating the model's robust self-adaptive optimization capability.

4.3. Impact of objective function weighting factors on optimization effectiveness

All simulations were conducted with the coal consumption weight factor p fixed at 0.95, based on standard coal pricing of 1000 CNY/t. This parameter remains fundamentally dynamic, intrinsically linked to fuel cost fluctuations that directly influence gradient optimization trajectories for layered air distribution and combustion stoichiometry adjustments. In conventional control systems, oxygen feedback control and manual adjustments are implemented as post-AGC optimization steps. This approach lacks explicit prioritization between boiler efficiency and NO_x concentration, potentially causing counteractive interactions among control parameters. Operational practices, however, prioritize CCR due to its significant impact on costs and efficiency. As illustrated in Fig. 11, a comparative analysis of unweighted optimization (CCR + NO_x) and weighted multi-objective optimization (J_{MESC}) reveals distinct outcomes. Without weighting factors, the unweighted strategy under high CCR-low NO_x conditions exhibits suboptimal performance, resulting in a 6.54 % increase in overall consumption. The comprehensive objective function mitigates this limitation by strategically allocating optimization efforts toward cost-sensitive targets, demonstrating that bias-aware optimization is pragmatically advantageous for CFPP.

To explore the impact of the weight factor p on the model's optimization performance, a series of experiments were conducted starting from an initial condition of high CCR and high NO_x. Different fuel-price multipliers (0.6, 0.8, 1.0, 1.2, 1.4) were applied in each experiment, while keeping the multi-objective optimization process the same. As the fuel price increases, the weight factor p for CCR also increases. Consequently, the decrease in CCR becomes more pronounced, while the reduction in NO_x concentration diminishes. This is because the composite objective function J_{MESC} places greater emphasis on CCR changes, leading the algorithm to prioritize CCR reduction, as shown in Fig. 12.

Operational implementation requires meticulous p calibration through continuous fuel market analysis integrated with combustion condition diagnostics and optimization target prioritization.

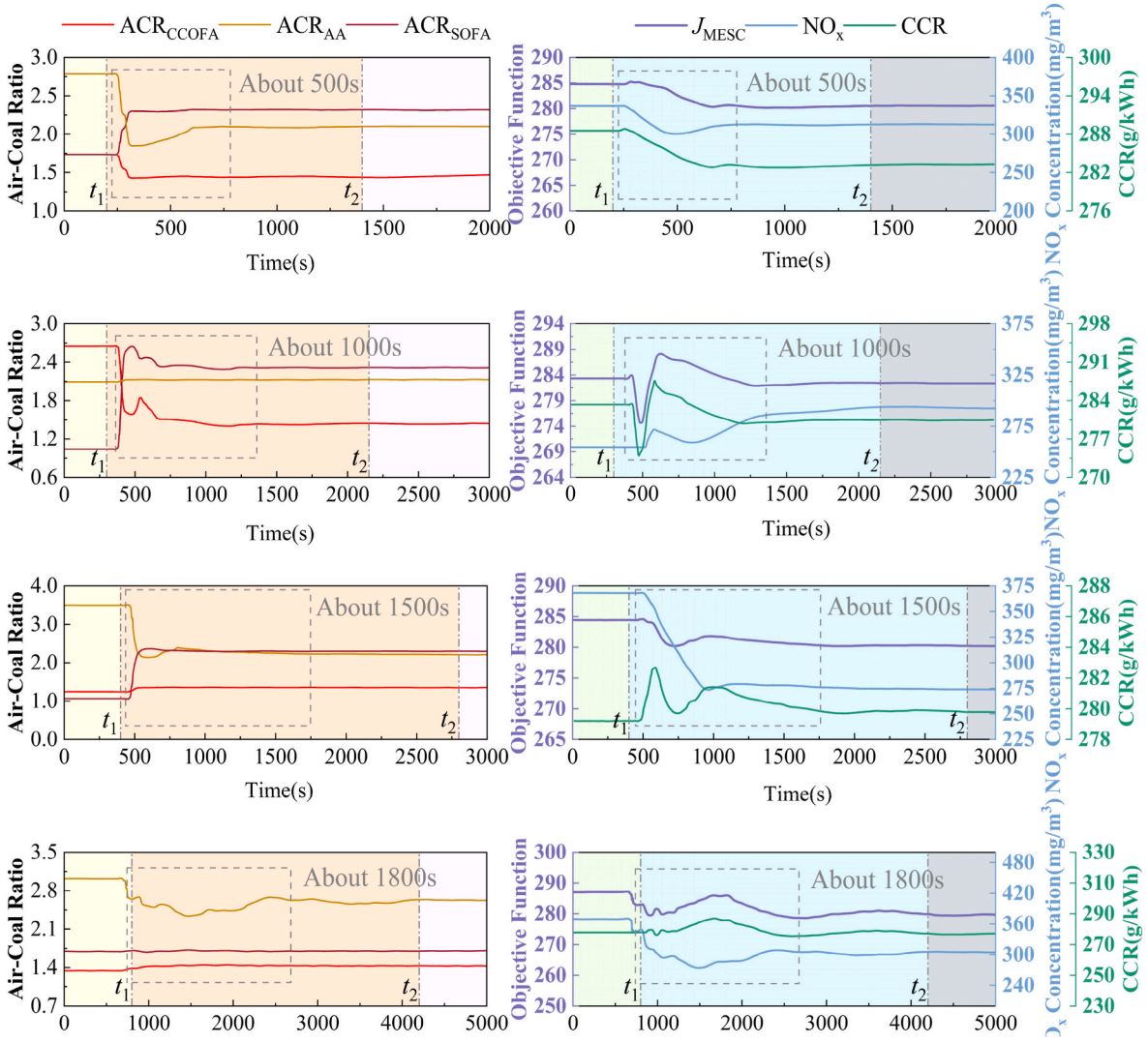

Fig. 9. Optimization control process for
(a) high CCR and high NO_x conditions (b) high CCR and low NO_x conditions
(c) low CCR and high NO_x conditions (d) coal quality disturbance condition.

Table 3
Multi-input optimization effects for high CCR and high NO_x initial condition.

	Load (MW)	ACR_{AA}	ACR_{CCOFA}	ACR_{SOFA}	NO_x (mg/m^3)	CCR (g/kWh)	J_{MESC}
IC	1000	2.8	1.75	1.75	337.65	284.70	287.35
OC	1000	2.12 (−24.29 %)	1.45 (−17.14 %)	2.33 (+33.14 %)	312.61 (−7.42 %)	280.54 (−1.46 %)	282.14 (−1.81 %)

Table 4
Multi-input optimization effects for high CCR and low NO_x initial conditions.

	Load (MW)	ACR_{AA}	ACR_{CCOFA}	ACR_{SOFA}	NO_x (mg/m^3)	CCR (g/kWh)	J_{MESC}
IC	1000	2.10	2.66	1.05	254.34	283.36	281.91
OC	1000	2.13 (+1.43 %)	1.44 (−45.86 %)	2.31 (+120 %)	292.37 (+14.95 %)	280.47 (−1.02 %)	281.07 (−0.30 %)

Table 5
Multi-input optimization effects for low CCR and high NO_x initial conditions.

	Load (MW)	ACR_{AA}	ACR_{CCOFA}	ACR_{SOFA}	NO_x (mg/m^3)	CCR (g/kWh)	J_{MESC}
IC	1000	3.50	1.26	1.09	366.90	280.09	284.41
OC	1000	2.22 (−36.57 %)	1.37 (+8.73 %)	2.31 (+111.93 %)	273.45 (−25.47 %)	280.54 (+0.16 %)	280.19 (−1.48 %)

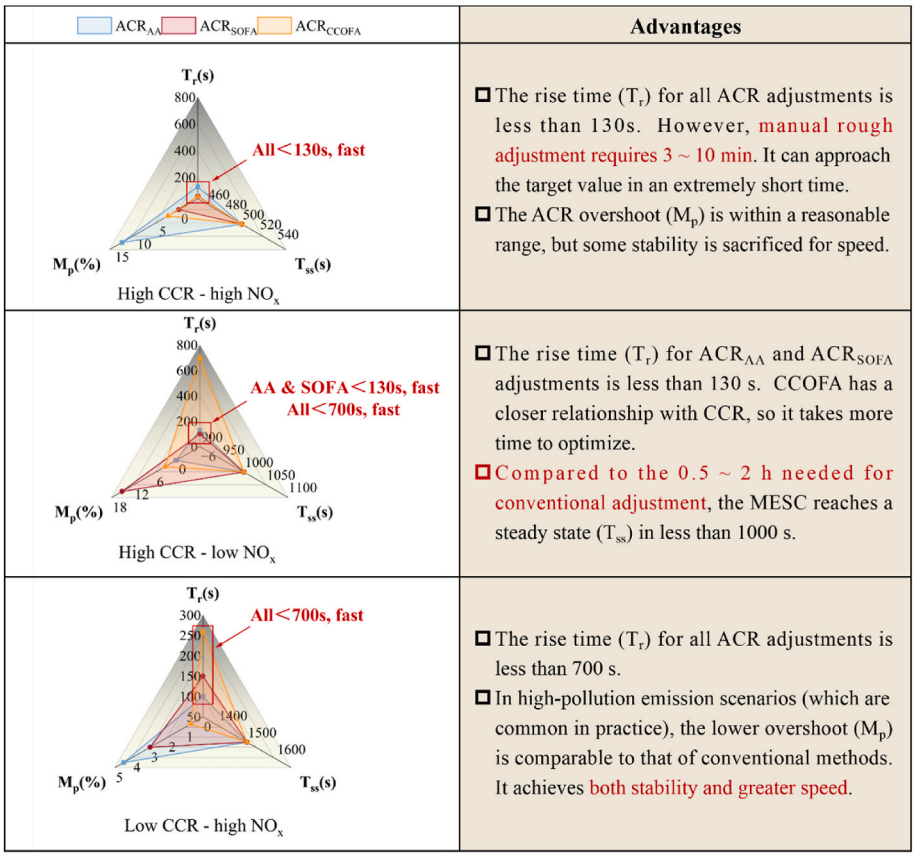

Fig. 10. Comparative analysis of MESC performance with traditional control system.

Table 6
Overshoot, rise time and settling time of ACR across three scenarios.

	High CCR - high NO_x			High CCR - low NO_x			Low CCR - high NO_x		
	AA	SOFA	CCOFA	AA	SOFA	CCOFA	AA	SOFA	CCOFA
T_r (s)	130	60	58	130	100	700	100	150	260
T_{ss}(s)	500	500	500	1000	1000	1000	1500	1500	1500
M_p(%)	13.2	0.3	2.8	0.5	15.2	3.5	4.5	3.0	0.7

5. Conclusion

This study developed and validated a multi-input extremum seeking control (MESC) algorithm based on a Simulink-APROS closed-loop control architecture to enhance the future adaptability of boiler systems. To evaluate the control optimization effectiveness, the impacts of load tracking capability during flexible operation, optimization performance in complex scenarios, and fuel economy considerations were systematically investigated. The MESC algorithm demonstrated strong robustness against external disturbances and rapid self-optimization capability in challenging initial conditions. The main conclusions are as follows.

1) The proposed MESC algorithm demonstrates effective load-following performance within the 1000 - 900 MW flexible operation range. Initial condition tests reveal a 1.53 % reduction in the comprehensive objective function (J_{MESC}) and a 27 % decrease in NO_x concentration. During load variations, the algorithm rapidly converges to near-optimal setpoints, outperforming conventional control strategies.
2) Through dynamic adjustments of three-layer ACR for stratified air distribution optimization, the algorithm intelligently identified optimization directions under scenarios such as combustion temperature anomalies, start-stop phases and coal quality disturbances. This resulted in continuous J_{MESC} reduction and rapid convergence to optimal values while dynamically adapting to real-time boiler feedback.
3) The MESC algorithm demonstrates exceptional rapid response capabilities, optimizing all air-coal ratios near optimal values within 700 s, while achieving the majority of optimization targets within 150 s, with overshoot maintained within acceptable limits.
4) Weighting factor analysis revealed that rising coal prices significantly elevate the optimization priority of carbon conversion rate (CCR), suggesting the need for a dynamic weight adjustment mechanism to balance economic and environmental objectives.

CRediT authorship contribution statement

Tianyu Zhou: Writing – original draft, Visualization, Software, Methodology, Data curation. **Chao Yang:** Validation, Software, Data curation. **Lijie Wang:** Writing – review & editing, Investigation. **Yifan Wang:** Writing – review & editing, Investigation. **Can Zhou:** Resources. **Xuesen Pu:** Resources. **Zhongcai Zhang:** Investigation. **Lingxiao Kong:** Investigation. **Zimu Dong:** Investigation. **Libin Yu:** Software. **Chang Tan:** Data curation. **Chenghang Zheng:** Writing – review & editing, Funding acquisition, Conceptualization. **Xiang Gao:** Funding acquisition, Conceptualization.

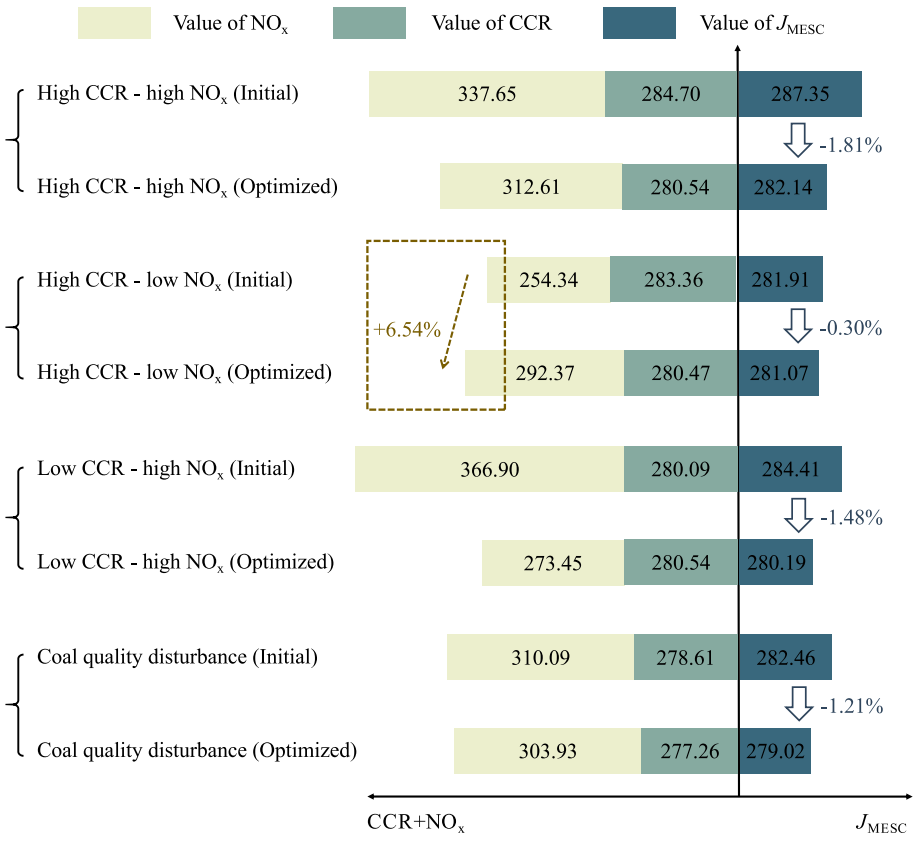

Fig. 11. The MESC framework directs optimization efforts toward cost-efficiency priorities, outperforming conventional control systems.

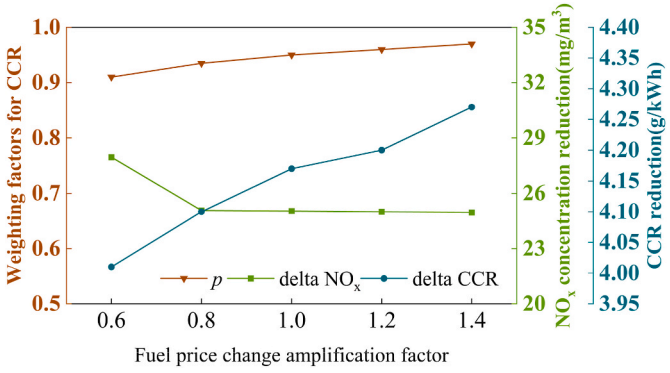

Fig. 12. Impact of different fuel prices on optimization effectiveness.

Declaration of competing interest

The authors declare that they have no known competing financial interests or personal relationships that could have appeared to influence the work reported in this paper.

Acknowledgments

This work was supported by the National Natural Science Foundation of China (42341208), the Pioneer and Leading Goose R&D Program of Zhejiang (2023C03008) (2025C01149).

Data availability

Data will be made available on request.

References

[1] IEA, World. Energy outlook. Paris: IEA; 2024. https://www.iea.org/reports/world-energy-outlook-2024.
[2] H. T. Peng, D. Zhang, J. T. Zhong, L. F. Guo, S. Y. Guo, J. L. Huang, D.Y. Wang, C. H. Miao, X. L. Zhang, X. Y. Zhang, A representative CO2 emissions pathway for China toward carbon neutrality under the Paris Agreement's 2°C target, Adv Clim Change Res , 14(6), 941–951.
[3] Hentschel J, Zindler H H, Spliethoff H. Modelling and transient simulation of a supercritical coal-fired power plant: dynamic response to extended secondary control power output. Energy 2017;137:927–40.
[4] Hubel S, Andrén Mt Meinke, Wedding C, Nocke J, Gierow C, et al. Modelling and simulation of a coal-fired power plant for start-up optimization. Appl Energy 2017; 208:319–31.
[5] Krstic M, Teel A R, et al. Extremum seeking control for nonlinear uncertain systems: a tutorial. In Proceedings of the 2013 American control conference (pp. 123–135). Washington, DC, USA: IEEE.
[6] Zhang Q, Dong J, Chen H, Feng F, Xu G, Wang X, et al. Dynamic characteristics and economic analysis of a coal-fired power plant integrated with molten salt thermal energy storage for improving peaking capacity. Energy 2024;290:130132.
[7] Wang W, Liu J, Zeng D, Fang F, Niu Y. Modeling and flexible load control of combined heat and power units. Appl Therm Eng 2020;166:114624.
[8] Chen C, Zhao C, Liu M, Wang C, Yan J. Enhancing the load cycling rate of subcritical coal-fired power plants: a novel control strategy based on data-driven feedwater active regulation. Energy 2024;312:133627.
[9] Esmaeili M, Moradi H. Robust & nonlinear control of an ultra-supercritical coal-fired once-through boiler-turbine unit in order to optimize the uncertain problem. Energy 2023;282:128312.
[10] B. Dai, F. Wang, Y. Chang, F. Chu, S. Song, Process model-assisted optimization control method based on model predictive control and deep reinforcement learning for coordinated control system in coal-fired power unit, IEEE Trans Autom Sci Eng , 22(1), 228–239.
[11] Zhu Y, Zhang K, Zhu Y, Jiang P, Zhou J. Development of a three-term MPC and its application to an ultra-supercritical coal fired power plant. Control Eng Pract 2024; 143:105787.
[12] Muhammad Ashraf W, Uddin Ghulam Moeen, Ahmad Hassan Afroze, Jamil Muhammad Ahmad, Tariq Rasikh, Shahzad Muhammad Wakil, Dua Vivek. Artificial intelligence enabled efficient power generation and emissions reduction underpinning net-zero goal from the coal-based power plants. Energy Convers Manag 2022;268:116025.
[13] Z. Cui, H. Jing, D. Wang, W. Chen, Y. Niu, Dynamic characterization and predictive control of the steam-molten salt heat exchanger in charging process , Energy, 321, 135523.

[14] P. Liao, X. Wu, M. Wang, Intelligent scheduling and flexible operation for the commercial-scale coal-fired power plant integrated with post-combustion carbon capture, IFAC-PapersOnLine , 55(9), 553–558.
[15] Yang C, Guo W, Shao Y, Lin Y, Pu X, Wang Y, Zheng C, Ding Y, Fan H, Zhu Y, Gao X. Two-timescale nonlinear model predictive control for flexible operation of coal-fired power plant with post combustion CO2 capture system. Appl Therm Eng 2024;256:124139.
[16] Kusiak A, Song Z. Combustion efficiency optimization and virtual testing: a data-mining approach. IEEE Trans Ind Inf 2006;2(3):176–84.
[17] Shi Y, Zhong W, Chen X, Yu A, Li J. Combustion optimization of ultra supercritical boiler based on artificial intelligence. Energy 2019;170:804–17.
[18] Echi S, Bouabidi A, Driss Z, Abid MS. CFD simulation and optimization of industrial boiler. Energy 2019;169:105–14.
[19] Liu X, Bansal R. Integrating multi-objective optimization with computational fluid dynamics to optimize boiler combustion process of a coal-fired power plant. Appl Energy 2014;130:658–69.
[20] Leblanc M. Sur l'electrification des chemins de fer au moyen de courants alternatifs de frequence elevee. Revue Generale de l'Electricite 1922;12(8):275–7.
[21] M. Krstic, Performance improvement and limitations in extremum seeking control, Syst Control Lett 39(5): 313–326.
[22] D. Nesic, Extremum seeking control: convergence analysis, Eur J Control , 15(3–4): 331–347.
[23] Zhang C, Ordonez R. Numerical optimization-based extremum seeking control with application to ABS design. IEEE Trans Automat Control 2007;52:454–67.
[24] Nwesaty W, Bratcu AI, Hably A. Extremum seeking control techniques applied to photovoltaic systems with multiodal power curves, international conference on renewable energy research and applications (ICRERA. 2013.
[25] Rodrigues D, Amrhein M, Billeter J, Bonvin D. Fast estimation of plant steady state for imperfectly known dynamic systems, with application to real-time optimization. Ind Eng Chem Res 2018;57:3699–716.
[26] Chen C, Jia M, You F, Wang F, Kou W. A new modifier adaptation methodology for real-time optimization,. Trans Inst Meas Control 2018;40:1320–7.
[27] Marchetti AG, Chachuat B, Bonvin D. Modifier-adaptation methodology for real-time optimization. Ind Eng Chem Res 2009;48:6022–33.
[28] Garcia CE, Morari M. Optimal operation of integrated processing systems. part I: open-loop on-line optimizing control. AIChE J 1981;27:960–8.
[29] Zhu Y, Yang C, Chen X, Zhou J, Zhao J. Identification-based real-time optimization and its application to power plants. Control Eng Pract 2022;123:105160.
[30] Marjanovic A, Krstic M, Djurovic Z, Kvascev G, Papic V. Combustion distribution control using the extremum seeking algorithm. European Workshop on Advanced Control and Diagnosis 2014;570:52001.
[31] Sharma Shubhkirti, Kumar Vijay. A comprehensive review on multi-objective optimization techniques: past, present and future,. Arch Comput Methods Eng 2022;29:5605–33.
[32] Jiang D, Dong Z. Dynamic matrix control for thermal power of multi-modular high temperature gas-cooled reactor plants. Energy 2020;198:117386.
[33] Wu X, Shen J, Li Y, Wang M, Lawal A. Flexible operation of post-combustion solvent-based carbon capture for coal-fired power plants using multi-model predictive control: a simulation study. Fuel 2018;220:931–41.
[34] Wang B, Ma H, Ren S, Si F. Effects of integration mode of the molten salt heat storage system and its hot storage temperature on the flexibility of a subcritical coal-fired power plant. Energy Storage 2023;58:106410.
[35] Li B, Cao Y, He T, Si F. Thermodynamic analysis and operation strategy optimization of coupled molten salt energy storage system for coal-fired power plant. Appl Therm Eng 2024;236:121702.
[36] Jae O, Chae, Chun Young N. Effect of two-stage combustion on NO_x emissions in pulverized coal combustion. Fuel 1990;70:703–7.
[37] Rees DP, Smoot LD, Hedman PO. Nitrogen oxide formation inside a laboratory pulverized coal combustor eighteenth international symposium on combustion. Pittsburgh: The Combustion Institute; 1981. p. 1305–12.
[38] Wang H, Yeung S, Krstic M. Experimental application of extremum seeking on an axial-flow compressor. IEEE Trans Control Syst Technol 2000;8:300–9.
[39] Krstic M, Wang HH. Stability of extremum seeking feedback for general nonlinear dynamic systems. Automatica 2000;36:595–601.